THE JOURNAL OF PHYSICAL CHEMISTRY B

Article

pubs.acs.org/JPCB

Vibrational Signatures of Cation−Anion Hydrogen Bonding in Ionic Liquids: A Periodic Density Functional Theory and Molecular Dynamics Study

Anirban Mondal and Sundaram Balasubramanian*

Chemistry and Physics of Materials Unit, Jawaharlal Nehru Centre for Advanced Scientific Research, Bangalore 560 064, India

Supporting Information

ABSTRACT: Hydrogen bonding in alkylammonium based protic ionic liquids was studied using density functional theory (DFT) and ab initio molecular dynamics (AIMD) simulations. Normal-mode analysis within the harmonic approximation and power spectra of velocity autocorrelation functions were used as tools to obtain the vibrational spectra in both the gas phase and the crystalline phases of these protic ionic liquids. The hydrogen bond vibrational modes were identified in the 150−240 cm^{-1} region of the far-infrared (far-IR) spectra. A blue shift in the far-IR mode was observed with an increasing number of hydrogen-bonding sites on the cation; the exact peak position is modulated by the cation−anion hydrogen bond strength. Sub-100 cm^{-1} bands in the far-IR spectrum are assigned to the rattling motion of the anions. Calculated NMR chemical shifts of the acidic protons in the crystalline phase of these salts also exhibit the signature of cation−anion hydrogen bonding.

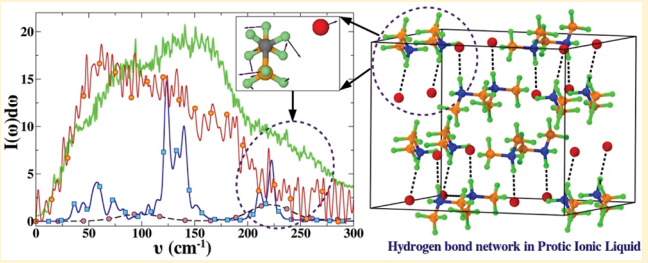

INTRODUCTION

Among the multitude of interactions prevalent in molten salts (ionic liquids), the predominant one is electrostatic. Coulombic interactions lead to strong binding energies between ions of the order of 500 kJ mol^{-1} or more.[1] Thus, most inorganic molten salts are found to be in the solid state at ambient conditions. However, room temperature ionic liquids (RTILs) are a class of molten salts which have melting points below 100 °C. An important subset of RTILs are protic ionic liquids (PILs), which can be synthesized by combining an equimolar amount of a Brønsted acid and a Brønsted base.[2−7] PILs contain both proton donor and acceptor sites which enable the formation of an extended hydrogen-bonded network,[8] a feature that distinguishes PILs from their aprotic counterparts. Thus, PILs have also served as a model to study such networks in the liquid state.[9−19] In recent years, they have attracted much attention as proton-conducting electrolytes for fuel cells due to their high proton-conductivity, thermal stability, and low vapor pressure.[20−25]

Ionic motions in ILs have been characterized by a variety of experimental methods.[19,26−37] In a molten salt, the cation rattles within a cage formed by the anions and vice versa. The rattling frequency is typically in the far-infrared (far-IR) region and can be studied using vibrational spectroscopy. It carries the signature of cation−anion interactions; the band position, although strictly related to the curvature of the potential energy surface, is also usually correlated with the strength of the interaction. Naturally, hydrogen-bonded ion partners exhibit a far-IR band at higher wave numbers than ones which do not.[38] Many intermolecular interactions contribute to this region of frequency, making it difficult to distinguish their contributions properly. Some research groups have suggested that long-range electrostatic interactions contribute to these bands rather than hydrogen bonding.[39,40] Sarangi et al.[15] proposed that the low frequency band arises primarily from interionic interactions and demonstrated that short-range interactions alone can reproduce it. Recently, Ludwig et al. have studied the far-IR spectra of PILs such as tetramethylammonium nitrate and trimethylammonium nitrate.[8] In $[Me_3NH][NO_3]$, they observed a distinct vibrational mode at 171 cm^{-1} which was not present in $[Me_4N][NO_3]$. They have also performed zero temperature, density functional theory (DFT) calculations of small clusters of neutral ion pairs in the gas phase. Combining these with NMR data, they concluded that this band represents vibrations associated with anion−cation interaction and can specifically be assigned to the $^{+}N-H\cdots NO_3^{-}$ hydrogen bond stretching mode. Hayes et al. studied hydrogen bonding in various ammonium ion based PILs using neutron diffraction.[41] Two types of H-bond were observed, one with a short H-bond distance (1.6−1.7 Å) and largely linear. The other one had a longer H-bond distance (2.4−2.6 Å) and was bent, causing the ionic liquid to melt at a lower temperature. Fumino et al. have combined far-IR vibrational spectroscopy with ab initio and DFT calculations to investigate cation−anion interactions in protic ionic liquids in terms of hydrogen bonding.[42−45] They suggested that the vibrational band representing the cation−anion interaction can be identified from other low frequency vibrational modes. While ab initio quantum chemical or DFT calculations have

Received: November 13, 2014
Revised: January 12, 2015
Published: January 14, 2015

DOI: 10.1021/jp5113679
J. Phys. Chem. B 2015, 119, 1994−2002

been performed on ion pair clusters (in the gas phase) to interpret experimental observations, it is imperative that condensed phase vibrational spectra too are explored theoretically, which, to our knowledge, has not been attempted yet.

In general, while quantum chemical calculations are carried out in the gas phase and empirical potential based molecular dynamics (MD) simulations in the condensed phase, ab initio molecular dynamics simulations provide a route to study intermolecular vibrations in condensed systems with little built-in empiricism. Here, our main objective is to study the crystalline states of ionic liquids wherein the coordination environment of an ion is quite similar to that in bulk ionic liquids. We have carried out Hessian calculations (using periodic DFT as well as force field) of the crystalline states of three alkylammonium based ionic liquids, dimethylammonium bromide ($[(CH_3)_2NH_2][Br]$), trimethylammonium bromide ($[(CH_3)_3NH][Br]$), and tetramethylammonium bromide ($[(CH_3)_4N][Br]$). Results from these simulations are reinforced by quantum chemical calculations of ion pairs and of ion pair dimers in the gas phase. These calculations are also augmented by calculations of NMR chemical shifts of hydrogen atoms obtained from crystalline and gas phase ion pair calculations. Empirical force field based MD simulations have also been employed to compute the power spectrum of the crystalline form of these ionic liquids.

The work is divided into three parts. This Introduction is followed by details of simulations employed to calculate the vibrational spectra and NMR chemical shifts. A subsequent section is devoted to description of the results. The last section presents a summary.

METHODOLOGY AND SIMULATION DETAILS

Isolated ion pairs of the three alkylammonium salts are shown in Figure 1.

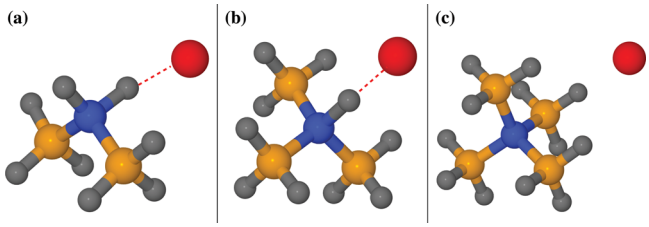

Figure 1. Optimized geometries of ion pairs of three alkylammonium salts obtained at the MP2/aug-cc-pvdz level of theory: (a) $[(CH_3)_2NH_2][Br]$, (b) $[(CH_3)_3NH][Br]$, and (c) $[(CH_3)_4N][Br]$. Color scheme: nitrogen, blue; carbon, orange; hydrogen, gray; bromine, red. The dotted line is the hydrogen bond between cation and anion.

Gas Phase. *Calculations Using Atom-Centered Basis Sets.* Geometries and vibrational spectra of ion pairs of these salts in gas phase were obtained using the Gaussian09 code.[46] In order to have a complete description of electron correlation, geometry optimizations were performed at the MP2/aug-cc-pvdz level of theory. Gaussview[47] was used to model the initial geometries. Optimization was performed by employing the keywords "opt= verytight" and "scf=verytight". Furthermore, an ultrafine grid was used in the DFT calculations. Normal-mode calculations of these systems at the harmonic level showed no imaginary frequencies, indicating that they were indeed at a minimum. We have also studied clusters of two ion pairs for all of these salts at the same level of theory as mentioned earlier.

Calculations Using Plane-Wave Basis Sets. DFT calculations for isolated ion pairs were performed using the CPMD-3.13.2 package.[48] The energy and density cutoffs were 150 and 900 Ry, respectively. Norm conserving Troullier–Martins pseudopotentials[49] were used to account for the effect of all of the core electrons and of the nucleus on the valence electrons. Exchange and correlation effects were treated through the Perdew, Burke, and Ernzerhof (PBE) functional.[50] The effect of van der Waals interactions (vdW) was considered through Grimme's method.[51] Optimizations under isolated conditions were carried out in a cubic box of length 12 Å, and the Poisson equation was solved using the Hockney method.[52] The gradient on the wave functions and on the nuclear positions were optimized with convergence criteria of 10^{-7} and 10^{-5} (au), respectively. The minimized structure was used to obtain the vibrational spectrum.

Crystalline Phase. *Periodic DFT Calculations.* Initial cell parameters and atom positions were taken from the Cambridge Crystal Structure Database.[53−55] A description of all of the systems studied here is provided in Table S1 of the Supporting Information. Other details of the calculations are the same as those discussed in DFT calculations for ion pairs. Each of these systems was optimized by varying the cell parameters and coordinates iteratively until the energy minimum was found. Calculated cell parameters differed by less than 0.5% of their experimental values (Table S2 of the Supporting Information). Forces on atoms were optimized with a convergence criterion of 10^{-5} au. Normal-mode analysis within the harmonic approximation was carried out on the final geometries.

Classical MD Simulations. Classical molecular dynamics simulations of crystalline phases of these salts have been carried out using LAMMPS.[56] Interaction parameters to model the PILs have been taken from the work of Canongia Lopes and Pádua.[57] The simulations were performed in the canonical ensemble using the Nosé–Hoover thermostat.[58] Equations of motion were integrated using the velocity Verlet algorithm with a time step of 1 fs. All C–H covalent bonds were constrained using the SHAKE algorithm as implemented in LAMMPS.[56] The ewald/disp solver was used to calculate the long-range interactions with a precision of 10^{-5}. The real space cutoff distance was 11 Å. Each system was equilibrated for 5 ns (in *NPT* ensemble) which was followed by 10 ns production run in the *NVT* ensemble. Atom coordinates were stored every 100 ps to obtain 100 snapshots for each PIL. Details of simulation cell parameters and simulation conditions are described in Table S3 of the Supporting Information.

Energy minimizations were performed on the 100 configurations selected from the classical MD trajectory for each ionic liquid using the conjugate gradient method in LAMMPS. A normal-mode analysis (NMA) code developed earlier within our group was used to calculate the Hessian matrix of the potential energy with respect to the atom coordinates.[59] While the eigenvalues of the Hessian are related to frequencies, the eigenvectors correspond to atomic displacements in a mode. The frequency spectrum was calculated using a bin width of 2 cm^{-1} and was averaged over the results for the 100 quenched configurations.

We have also calculated the vibrational density of states (VDOS) from the MD trajectory as the Fourier transform of the time autocorrelation functions of the atomic velocities (VACF). This can be expressed as

DOI: 10.1021/jp5113679
J. Phys. Chem. B 2015, 119, 1994−2002

$$I(\omega) = \frac{1}{k_B T} \sum_j m_j \left[\frac{1}{2\pi} \int_{-\infty}^{\infty} \exp(-i\omega t) \langle \mathbf{v}_j(0) \cdot \mathbf{v}_j(t) \rangle \, dt \right] \quad (1)$$

where $\mathbf{v}_j(t)$ is the velocity of atom type j at time t. To calculate this VACF, a separate MD trajectory was generated for a duration of 100 ps and atomic velocities were stored at each time step.

Ab Initio MD Simulations. Born−Oppenheimer molecular dynamics (BOMD) simulations of crystalline phases of these salts were performed using CPMD-3.13.2 software.[48] The temperature of ions was set to that value at which the crystal structures were determined experimentally (143, 100, and 293 K for $[Me_2NH_2][Br]$, $[Me_3NH][Br]$, and $[Me_4N][Br]$, respectively). A Nosé−Hoover chain thermostat[60] was used with a coupling constant of 1500 cm^{-1}. Equations of motion were integrated with a time step of 15 au. For these simulations, an energy cutoff of 85 Ry was used to expand the wave function, and four times this value was used for the electronic density. The systems were equilibrated for 2 ps followed by production runs for 12 ps. Velocity autocorrelation functions of the ions were calculated, and VDOS was obtained from the Fourier transform of this function.

All of the systems were visualized using Mercury,[61] VMD,[62] and Jmol.[63] Atomic displacements were visualized in Jmol[63] for the assignment of modes.

NMR Chemical Shift. *Gas Phase.* Geometries of ion pairs were optimized at the B3LYP/6-311++G(d,p) level of theory using Gaussian09[46] software. The quenched geometries were used to obtain ^1H NMR chemical shielding at the same level of theory. Chemical shifts were also calculated for the crystals using the periodic DFT code CPMD-3.13.2. Chemical shift calculations for gas phase ion pairs obtained from CPMD-3.13.2. were benchmarked against those from Gaussian in Table S5 of the Supporting Information. The $\delta(^1H)$ values calculated using plane-wave basis sets is able to reproduce the chemical shifts obtained from atom-centered basis sets.

Crystalline Phase. NMR chemical shifts were also studied for the crystalline systems consisting of 1 unit cell. Geometry optimization was performed under periodic boundary conditions, with a convergence criterion of 10^{-4} au for the forces on atoms. In these calculations which employed the PBE functional,[50] an energy cutoff of 80 Ry was used for the wave function. NMR resonance frequencies were obtained using a method[64] that is implemented in CPMD. It has been proven to capture the effect of hydrogen bonding and has yielded results in good agreement with experiments.[63−68]

The shielding constant of tetramethylsilane (TMS) was used as reference; thus, $\delta(H) = \sigma(TMS) - \sigma(H)$, where $\sigma(TMS)$ is the shielding calculated for an isolated TMS molecule at the same level of theory.

RESULTS AND DISCUSSION

Gas Phase. Normal-mode analysis was performed for three alkylammonium salts in the gas phase. Frequencies which are present above 400 cm^{-1} can be attributed to intramolecular modes and hence are not of interest here. The calculated spectra exhibit bands at sub-200 cm^{-1} which are usually attributed to unspecific librational motions.[8] The far-infrared absorption band red shifts with decreasing propensity for the formation of a cation−anion hydrogen bond, i.e., from dimethyl based cation to the tetramethyl based one.

Vibrational spectra obtained at the MP2/aug-cc-pvdz level for an ion pair of $[(CH_3)_2NH_2][Br]$ showed a characteristic mode at 221 cm^{-1}, whereas, for $[(CH_3)_3NH][Br]$ and $[(CH_3)_4N][Br]$, it was present at 193 and 146 cm^{-1}, respectively. Harmonic frequencies obtained from gas phase calculations using the plane-wave basis set (i.e., within CPMD) were consistent with the values calculated with the localized basis set. The optimized geometries of ion pairs of these three alkylammonium salts are compared in Figure S1 of the Supporting Information. The distance between the acidic hydrogen atom of the cation and the bromide anion along with the interaction energy of these ion pairs are provided in Table S4 of the Supporting Information. The corresponding frequencies for the three ion pairs calculated with CPMD were found to be 212, 201, and 148 cm^{-1}, respectively. The calculated spectra (up to 300 cm^{-1}) of these alkylammonium salts are plotted in Figure 2. Harmonic frequencies for clusters

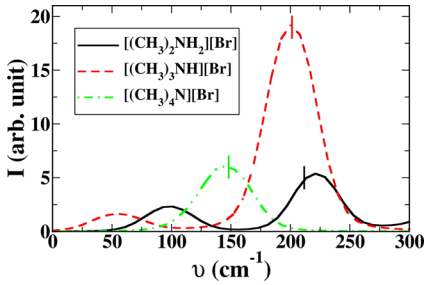

Figure 2. Far-IR spectra of different alkylammonium salts obtained from ion pair calculations at the MP2/aug-cc-pvdz level. Short vertical lines are values of frequencies obtained from DFT calculations of ion pairs using CPMD.

of two ion pairs of each of these salts were also calculated at MP2/aug-cc-pvdz level. A similar trend in frequencies in the low wavenumber region was observed with an increasing number of methyl groups on the cation; however, the frequencies were distinctly lower than those obtained for a single ion pair. Frequencies obtained for dimers of $[(CH_3)_2NH_2][Br]$, $[(CH_3)_3NH][Br]$, and $[(CH_3)_4N][Br]$ are 197, 181, and 144 cm^{-1}, respectively. The red shift in the frequencies with increasing numbers of ion pairs points to the necessity to study either large clusters in the gas phase (computationally forbidding) or adopt periodic DFT calculations.

We examine the data in terms of cation−anion hydrogen bonding. In $[Me_2NH_2][Br]$, there are two acidic protons on the nitrogen atom, whereas in $[Me_3NH][Br]$, only one such acidic hydrogen is present. In $[Me_4N][Br]$, there are no acidic protons, thus depriving it of any hydrogen-bonding interaction with the anion. Going from the dimethyl- to tetramethylammonium cation, the hydrogen bond formation ability decreases, which considerably influences the far-IR band position. The "inductive effect" also plays a crucial role here. The transmission of charge in a molecule through a chain of atoms by electrostatic induction is known as inductive effect, which can be either positive or negative in character. From the dimethyl to the tetramethyl group, the electron releasing character increases. This would lead to lesser charge transfer into the N−H antibonding orbital, as the electron density at ammonium nitrogen increases—indicating a weaker hydrogen bond. This leads to a red shift in the frequency of the intermolecular mode as the hydrogen bond weakens. Therefore, it is clear that the

DOI: 10.1021/jp5113679
J. Phys. Chem. B 2015, 119, 1994−2002

characteristic frequency band represents anion−cation interaction and can be assigned to the $^{+}N-H\cdots Br^{-}$ hydrogen bond. Visualization of the atomic displacements of these vibrational modes clearly indicates the H-bonding stretching characteristic as shown in Figure 3.

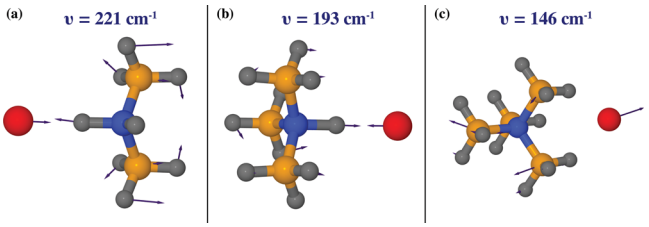

Figure 3. Interionic low frequency modes in ion pairs of (a) $[(CH_3)_2NH_2][Br]$, (b) $[(CH_3)_3NH][Br]$, and (c) $[(CH_3)_4N][Br]$ as studied through MP2/aug-cc-pvdz level calculations in the gas phase. The atomic displacement vectors are shown as arrows and are scaled by a factor for better visualization. Color scheme: nitrogen, blue; carbon, orange; hydrogen, gray; bromine, red.

Crystal Phase: DFT. Thus far, we discussed the far-IR vibrational modes of one ion pair in the gas phase. As mentioned earlier, condensed phase effects are significant and discernible in the far-IR region of the vibrational spectrum. Thus, we have performed Hessian calculations on the crystalline phase of these three salts as well. These intermolecular mode frequencies were found to be consistently higher than ones calculated for isolated ion pairs. A stick pattern of the calculated spectra for these salts is shown in Figure 4. A group of vibrational frequencies for dimethyl-,

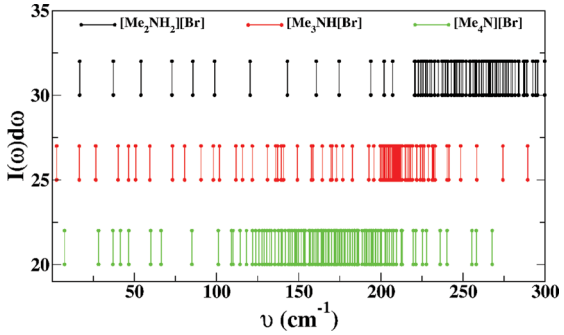

Figure 4. Stick pattern of calculated far-IR spectra obtained through Hessian calculations of crystalline (based on periodic DFT calculations) phases of alkylammonium ILs.

trimethyl-, and tetramethylammonium bromide are located around 248, 209, and 162 cm^{-1}, respectively. Thus, the trend observed in the gas phase vibrational analysis is present in the crystalline phase of these ammonium salts as well. In both sets of calculations, an increase in the number of H-bonding sites on the cation blue shifts the intermolecular vibrational mode. Atomic displacement vectors corresponding to a specific cation−anion vibrational mode at low wave numbers in the three different salts in their crystalline states are shown in Figure 5.

The interionic character of the modes at low frequencies for these alkylammonium salts have so far been examined through zero temperature Hessian calculations. In order to substantiate our observations, we have also performed finite temperature MD simulations of these salts in their crystalline states.

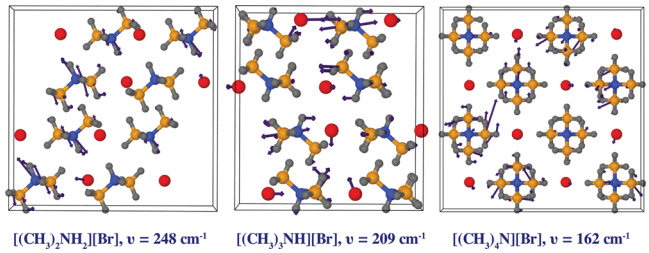

Figure 5. Interionic character of selected modes in crystalline alkylammonium salts calculated using periodic DFT calculations through a diagonalization of the Hessian within the harmonic approximation. Atomic displacement vectors are shown as arrows and are scaled by an arbitrary factor for clarity. Color scheme: nitrogen, blue; carbon, orange; hydrogen, gray; bromine, red.

Crystal Phase: Empirical Potential. As described in the earlier section, the VDOS were obtained from both NMA and the power spectrum of autocorrelation functions of atomic velocities from a classical MD (generated with empirical potential) trajectory. The density of states for the three crystals obtained from these two approaches are shown in Figure 6. Imaginary frequencies are shown in Figure S2 of the Supporting Information. The number and intensity of such imaginary frequencies are insignificant. A prominent feature around 200 cm^{-1} is observed for $[(CH_3)_2NH_2][Br]$ and $[(CH_3)_3NH][Br]$, which is absent in the spectrum of $[(CH_3)_4N][Br]$. Instead, we can clearly see a gap in the VDOS for $[(CH_3)_4N][Br]$. A similar, but narrower gap is observed for $[(CH_3)_3NH][Br]$. The VDOS for $[(CH_3)_2NH_2][Br]$ is devoid of such a gap.

Figure 7 displays atomic displacements of modes obtained by diagonalizing the Hessian determined via the empirical force field. The acidic protons (N−H) mainly contribute to the modes in the frequency range 200−240 cm^{-1} (Figure 7a) for $[(CH_3)_2NH_2][Br]$, while, for $[(CH_3)_3NH][Br]$, similar protons contribute to modes in the range of 185−200 cm^{-1} (Figure 7b).

The hydrogen bond network in the PILs are displayed in Figure 7c,d. Each bromide anion in $[(CH_3)_2NH_2][Br]$ forms hydrogen bonds with two acidic hydrogens, while, in $[(CH_3)_3NH][Br]$, it can form only one. The radial distribution function between bromide and the acidic hydrogen atom (N−H) obtained from the experimental crystal structure (single configuration) is shown in Figure S3 of the Supporting Information. The mean Br−H distance in $[(CH_3)_3NH][Br]$ is slightly larger than in $[(CH_3)_2NH_2][Br]$; as expected, the coordination number is 2 and 1 for $[(CH_3)_2NH_2][Br]$ and $[(CH_3)_3NH][Br]$, respectively. The atomic displacements obtained using NMA code in the region of 50−100 cm^{-1} are shown in Figure 8, and it can be seen that the bromide anions mainly contribute to the modes present in this range.

Crystal Phase: Ab Initio MD Simulations. The AIMD trajectory was used to calculate the autocorrelation function of the ion velocities, and the Fourier transform of this function yields the VDOS. The density of states for the three salts in their crystalline states obtained from finite temperature AIMD simulations are shown in Figure 9. Consistent with the results from Hessian calculations, the low frequency band red shifts as the number of NH protons is reduced. The trend in the position of the low frequency band observed in the Hessian calculations is also present in the VDOS of these salts in their crystalline states. Because $[(CH_3)_4N][Br]$ does not have any cation−anion hydrogen bonding, the low wavenumber peaks

DOI: 10.1021/jp5113679
J. Phys. Chem. B 2015, 119, 1994−2002

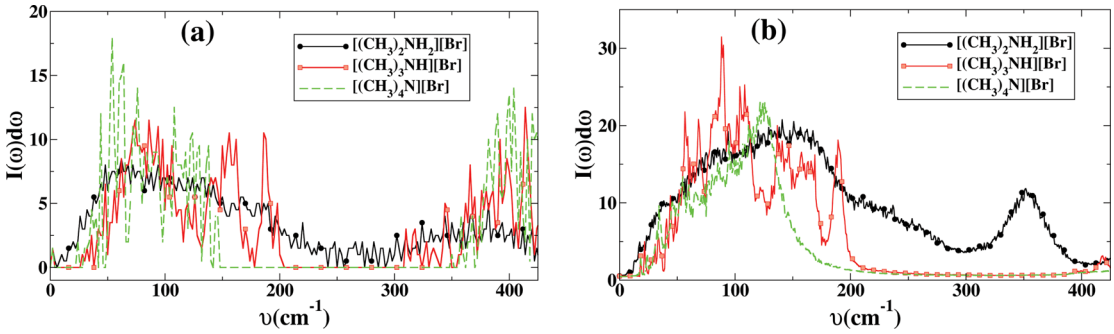

Figure 6. Comparison of the low frequency region of vibrational density of states (VDOS) obtained from (a) a normal-mode analysis (NMA) and (b) as the power spectrum of time autocorrelation functions of atomic velocities from a classical MD trajectory, for the three PILs in their crystalline states.

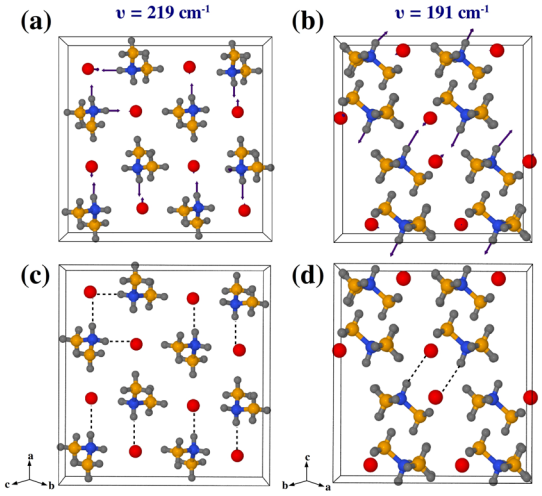

Figure 7. Interionic character of selected modes in crystalline alkylammonium salts calculated using NMA: (a) $[(CH_3)_2NH_2][Br]$ and (b) $[(CH_3)_3NH][Br]$. Atomic displacement vectors are shown as arrows and are scaled by an arbitrary factor for clarity. Hydrogen bond network in PILs: (c) $[(CH_3)_2NH_2][Br]$ and (d) $[(CH_3)_3NH][Br]$ as obtained from experimental crystal structure. Color scheme: nitrogen, blue; carbon, orange; hydrogen, gray; bromine, red.

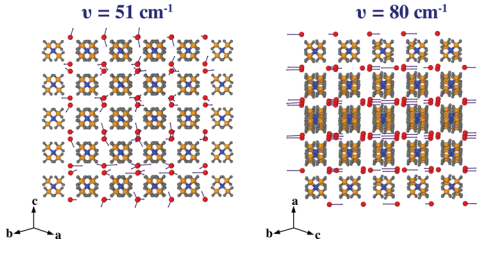

Figure 8. Interionic character of selected modes in crystalline $[(CH_3)_4N][Br]$ calculated using normal-mode analysis within a classical force field. Atomic displacement vectors are shown as arrows and are scaled by an arbitrary factor for clarity. Color scheme: nitrogen, blue; carbon, orange; hydrogen, gray; bromine, red.

are a signature of only electrostatic and other short-range interactions between the ions. The bands for $[(CH_3)_3NH][Br]$ and $[(CH_3)_2NH_2][Br]$ are modulated further by the cation−anion hydrogen bond. The influence of the cation−anion hydrogen bond is also reflected in the high wavenumber region (>3000 cm^{-1}). Due to the formation of more hydrogen bonds in $[(CH_3)_2NH_2][Br]$ than in $[(CH_3)_3NH][Br]$, the N−H covalent bond in $[(CH_3)_3NH][Br]$ was expected to be stronger

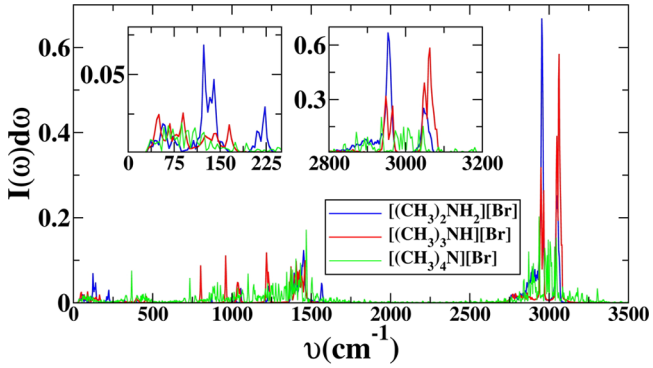

Figure 9. Power spectra of velocity autocorrelation function obtained from AIMD simulation of different alkylammonium salts in their crystalline states. Insets: (a) magnified low frequency region corresponding to cation−anion hydrogen bonding; (b) high frequency region of VDOS corresponding to C−H and N−H stretching vibrations.

than in $[(CH_3)_2NH_2][Br]$. Therefore, the N−H stretching frequency in $[(CH_3)_3NH][Br]$ can be expected to be present at a higher wavenumber compared to $[(CH_3)_2NH_2][Br]$. These observations are confirmed in Figure 9 which provides the VDOS in the high frequency region. In Figure 9, modes present around 2900 cm^{-1} correspond to the C−H stretching frequencies while N−H stretching vibrations are present around 3100 cm^{-1}.

The effect of a cation−anion hydrogen bond on the vibrational spectrum was analyzed further from the AIMD trajectories. The velocities of the acidic proton(s) that forms the hydrogen bond with the bromide anion were projected along the N−H···Br bond vector. The autocorrelation function of this component was analyzed through its Fourier transform. This quantity is thus the power spectrum specifically for the hydrogen bond stretching mode. A schematic of these calculations is provided in Figure 10 along with the corresponding spectra for $[(CH_3)_2NH_2][Br]$ and $[(CH_3)_3NH][Br]$. In $[(CH_3)_2NH_2][Br]$, the low wavenumber peak is present at around 220 cm^{-1} arising due to strong $^{+}N-H\cdots Br^{-}$ interaction. On the other hand, the weaker interaction between the same pair in $[(CH_3)_3NH][Br]$ results in a red shift in that mode, and the same is located at 165 cm^{-1}. The three methyl groups provide a large positive inductive effect, resulting in a less acidic NH proton (where the nitrogen atom is more electron rich) in $[(CH_3)_3NH][Br]$. On the contrary, the NH proton of $[(CH_3)_2NH_2][Br]$ is found to be more acidic in nature due to a less electron rich N center. A more acidic

DOI: 10.1021/jp5113679
J. Phys. Chem. B 2015, 119, 1994−2002

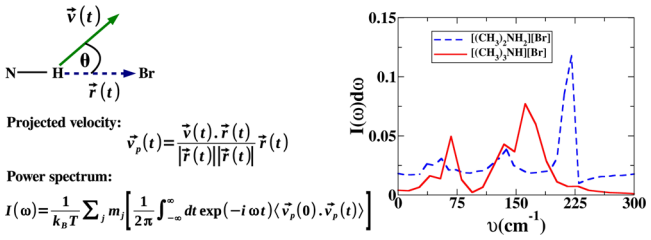

Figure 10. Left panel: Scheme of the projection of acidic hydrogen velocities along the cation−anion hydrogen bond axis. Right panel: Power spectra of velocity autocorrelation function of acidic hydrogen projected along the cation−anion hydrogen bond axis.

hydrogen atom interacts stronger with the bromide anion which results in a blue shift in the low frequency vibrational band in $[(CH_3)_2NH_2][Br]$. This analysis conclusively demonstrates these modes to possess hydrogen bond stretching character.

The presence and strength of hydrogen bonding in PILs was further investigated in terms of hydrogen bond length and angle. The distributions of hydrogen bond length and hydrogen bond angle in $[(CH_3)_2NH_2][Br]$ and $[(CH_3)_3NH][Br]$ were calculated from the AIMD trajectories and are compared in Figure 11. The mean hydrogen bond distance in $[(CH_3)_2NH_2]$-

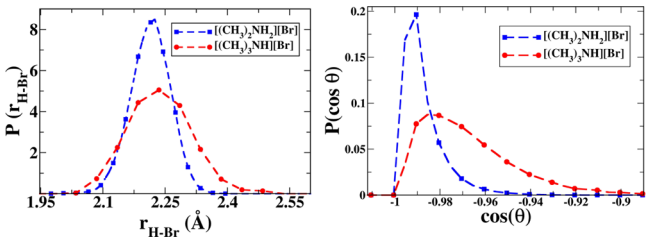

Figure 11. Normalized distribution of NH···Br bond length and N−H···Br angle in crystalline $[(CH_3)_2NH_2][Br]$ and $[(CH_3)_3NH][Br]$ calculated from the AIMD trajectory.

$[Br]$ is marginally shorter than in $[(CH_3)_3NH][Br]$. On the other hand, the difference in hydrogen bond angle was more prominent. In the case of $[(CH_3)_2NH_2][Br]$, the cation−anion hydrogen bond was found to be more linear, and the N−H···Br angle is close to 180°. However, the mean angle in $[(CH_3)_3NH][Br]$ is around 165°. Hence, these observations also suggest stronger intermolecular interaction in $[(CH_3)_2NH_2][Br]$ than in $[(CH_3)_3NH][Br]$.

$\delta(^1H)$ NMR. The NMR chemical shifts $\delta(^1H)$ in these alkylammonium salts were calculated both in the gas phase and in the crystalline phase. The calculations have also been carried out for chloride (Cl^-) and iodide (I^-) anion based salts in their gas phase for the sake of comparison. The chemical shifts for the salts are plotted against their corresponding (^+N−H··· anion) far-IR frequencies in Figure 12. As the ^+N−H···anion interaction increases, a blue shift in far-IR frequency is observed, with a corresponding increase in $\delta(^1H)$. The interaction strength is the highest for chloride which leads to a large NMR downfield proton chemical shift and high far-IR frequencies. On the other hand, iodide anion showed an upfield shift and a red shift in the far-IR frequency relative to chloride and bromide anions. The difference in the number of electron releasing groups in the two types of cations results in differences in the interaction strength and the $\delta(^1H)$ values. The $\delta(^1H)$ values obtained for the bromide based crystals are

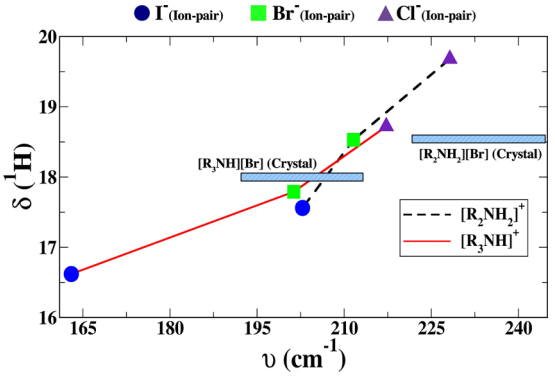

Figure 12. Chemical shifts $\delta(^1H)$ for the N−H proton plotted against ^+N−H···anion far-IR frequencies of alkylammonium salts in their gas phase. For crystalline systems, $\delta(^1H)$ values are plotted against a group of vibrational frequencies that correspond to the ^+N−H···anion interionic vibrational band (as depicted in Figure 4). Data presented here are obtained from CPMD code.[48]

comparable to those obtained for the corresponding ion pairs in the gas phase. Thus, at least as far as chemical shift values are concerned, gas phase calculations appear sufficient.

To examine further the hydrogen bond donor−acceptor properties in these PILs, the total electron density difference map was calculated using GaussView[47] and visualized in VMD.[62] The electron density of each fragment in the gas phase (cation and anion) at the MP2/aug-cc-pvdz level of theory was also calculated. The sum of the electron density of each fragment was then subtracted from the total electron density of the ion pair in the gas phase. This difference is shown in Figure 13.

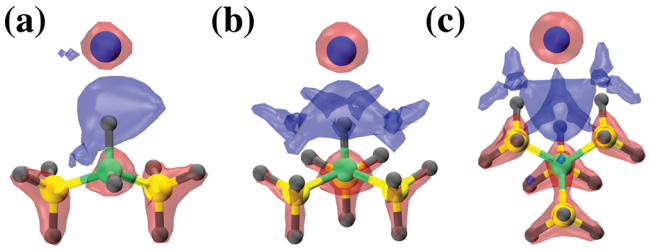

Figure 13. Electron density difference maps for (a) $[(CH_3)_2NH_2]$-$[Br]$, (b) $[(CH_3)_3NH][Br]$, and (c) $[(CH_3)_4N][Br]$.

In Figure 13, blue (red) represents the loss (gain) of electron density. In $[(CH_3)_2NH_2][Br]$ and $[(CH_3)_3NH][Br]$, the acidic hydrogen acts as the electron deficient center while the bromide anion acts as the electron rich center (hydrogen bond acceptor). The presence of these two centers with different electron densities can enable charge transfer between ions in these salts. The atomic charges of these salts in their crystalline states were calculated using the density-derived electrostatic and chemical (DDEC) charge partitioning method.[69,70] Details of these calculations have been described by us earlier.[71] The total ion charges were found to be ±0.647, ±0.658, and ±0.667 for $[(CH_3)_2NH_2][Br]$, $[(CH_3)_3NH][Br]$, and $[(CH_3)_4N][Br]$. Thus, the extent of charge transfer in these salts follows the same trend as the strength of interionic interactions.

Figure 14 summarizes the frequency spectra for $[(CH_3)_2NH_2][Br]$ obtained using the different techniques. The same for $[(CH_3)_3NH][Br]$ is shown in Figure S4 of the Supporting Information.

DOI: 10.1021/jp5113679
J. Phys. Chem. B 2015, 119, 1994−2002

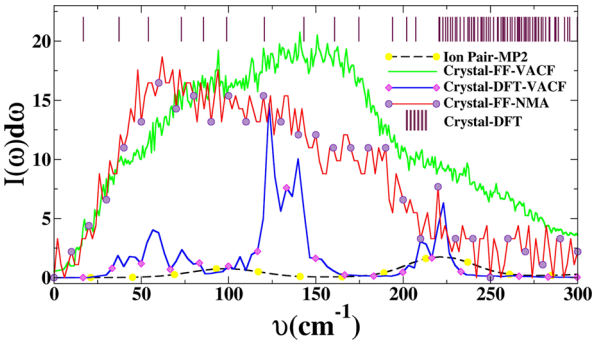

Figure 14. Frequency spectra of crystalline $[(CH_3)_2NH_2][Br]$ calculated through different methods. The spectra calculated from density functional theory within the harmonic approximation for an "ion-pair" and of a "crystal supercell" (stick pattern, marked Crystal-DFT) are shown for comparison. "Crystal-FF-VACF" and "Crystal-DFT-VACF" stand for the power spectrum of the velocity autocorrelation function calculated from classical MD and AIMD trajectories, respectively. "Crystal-FF-NMA" is the frequency spectrum obtained by performing NMA on configurations selected from the trajectory generated in classical MD simulation.

CONCLUSION

We have reviewed the far-infrared region of the vibrational spectrum of alkylammonium based protic ionic liquids using a set of computational techniques. Harmonic frequencies were calculated for isolated ion pairs as well as for the crystalline states of these salts. Both classical and ab initio molecular dynamics simulations were performed for three different PILs in their crystalline states. The time correlation function for ion velocities were used to obtain the vibrational power spectra of these crystals. Normal-mode analyses were also performed using the classical MD trajectory to obtain the vibrational density of states within the harmonic approximation.

We have observed distinct vibrational modes located in the 150−240 cm^{-1} region of the spectra, corresponding to near-neighbor cation−anion interactions. Vibrational analysis has provided rich information on the nature of these modes. Specifically, we find a blue shift in the far-IR mode with an increasing number of hydrogen-bonding sites on the cation. This frequency shift was related to the difference in interaction strength arising as a result of inductive effects caused by a different number of alkyl groups present on the cation. The difference in the strength of the cation−anion hydrogen bond was further probed with the help of geometrical parameters such as the hydrogen bond distance and hydrogen bond angle. In $[(CH_3)_2NH_2][Br]$, the hydrogen bond is more linear than in $[(CH_3)_3NH][Br]$, alluding to the former's strength. Such low frequency modes were also observed in ILs containing different anions such as $[CH_3SO_3]^-$, $[CF_3SO_3]^-$, $[NTf_2]^-$, and $[NO_3]^-$, etc., coupled with $[R_3NH]^+$ cation.[7,45] The position of the peak was found to be modulated by the interaction strength between ion pairs in these PILs. Such a modulation in the peak position with change in the interaction strength between ions was also observed in many spectroscopic investigations.[7,44,45] We have also examined the vibrational modes located below the 100 cm^{-1} region of spectra. The modes present in this region of spectra are mainly due to the rattling motions of bromide anions. Similar interionic modes of cations are observed in the range of 100−200 cm^{-1}.

Results from these vibrational analyses were further supported by NMR chemical shift values of acidic hydrogen atoms in different PILs. The $\delta(^1H)$ values are correlated with the characteristic low frequency peak positions. The hydrogen bond donor−acceptor properties were further examined through electron density difference maps. The charge transfer effects in the crystalline phase of these salts were probed through the DDEC/c3 charge partitioning method,[69,70] which predicts a fractional ion charge for all of these systems, and the values are consistent with trends exhibited by the position of the low frequency band in these PILs.

ASSOCIATED CONTENT

Supporting Information

Tables listing a summary of cell parameters of different crystalline systems, optimized cell parameters, information about the liquid systems studied for normal-mode analysis, distance between the acidic hydrogen atom of cation and bromide anion and interaction energies of PILs, and NMR chemical shift values and figures showing optimized geometries of ion pairs of PILs via different methods, imaginary modes in the power spectrum obtained from NMA calculations, site−site radial distribution functions, and frequency spectra calculated through different methods. This material is available free of charge via the Internet at http://pubs.acs.org.

AUTHOR INFORMATION

Corresponding Author

*E-mail: bala@jncasr.ac.in.

Notes

The authors declare no competing financial interest.

ACKNOWLEDGMENTS

We thank DST for support. S.B. thanks Sheikh Saqr Laboratory, JNCASR, for a senior fellowship. We thank the Centre for the Development of Advanced Computing (CDAC), Bangalore and CSIR-4PI, Bangalore where a part of the computations were carried out.

REFERENCES

(1) Zahn, S.; Bruns, G.; Thar, J.; Kirchner, B. What Keeps Ionic Liquids in Flow? *Phys. Chem. Chem. Phys.* **2008**, *10*, 6921−6924.
(2) Greaves, T. L.; Drummond, C. J. Protic Ionic Liquids: Properties and Applications. *Chem. Rev.* **2008**, *108*, 206−237.
(3) Bodo, E.; Postorino, P.; Mangialardo, S.; Piacente, G.; Ramondo, F.; Bosi, F.; Ballirano, P.; Caminiti, R. Structure of the Molten Salt Methyl Ammonium Nitrate Explored by Experiments and Theory. *J. Phys. Chem. B* **2011**, *115*, 13149−13161.
(4) Angell, C. A.; Byrne, N.; Belieres, J.-P. Parallel Developments in Aprotic and Protic Ionic Liquids: Physical Chemistry and Applications. *Acc. Chem. Res.* **2007**, *40*, 1228−1236.
(5) Xu, W.; Angell, C. A. Solvent-Free Electrolytes with Aqueous Solution-Like Conductivities. *Science* **2003**, *302*, 422−425.
(6) Stoimenovski, J.; Izgorodina, E. I.; MacFarlane, D. R. Ionicity and Proton Transfer in Protic Ionic Liquids. *Phys. Chem. Chem. Phys.* **2010**, *12*, 10341−10347.
(7) Fumino, K.; Wulf, A.; Ludwig, R. Hydrogen Bonding in Protic Ionic Liquids: Reminiscent of Water. *Angew. Chem., Int. Ed.* **2009**, *48*, 3184−3186.
(8) Fumino, K.; Reichert, E.; Wittler, K.; Hempelmann, R.; Ludwig, R. Low-Frequency Vibrational Modes of Protic Molten Salts and Ionic Liquids: Detecting and Quantifying Hydrogen Bonds. *Angew. Chem., Int. Ed.* **2012**, *51*, 6236−6240.
(9) Hunt, P. A.; Kirchner, B.; Welton, T. Characterising the Electronic Structure of Ionic Liquids: An Examination of the 1-Butyl-3-Methylimidazolium Chloride Ion Pair. *Chem.—Eur. J.* **2006**, *12*, 6762−6775.

DOI: 10.1021/jp5113679
J. Phys. Chem. B 2015, 119, 1994−2002

(10) Dommert, F.; Schmidt, J.; Qiao, B.; Zhao, Y.; Krekeler, C.; Delle Site, L.; Berger, R.; Holm, C. A Comparative Study of Two Classical Force Fields on Statics and Dynamics of [EMIM][BF_4] Investigated Via Molecular Dynamics Simulations. *J. Chem. Phys.* **2008**, *129*, No. 224501.
(11) Hunt, P. A.; Gould, I. R.; Kirchner, B. The Structure of Imidazolium-Based Ionic Liquids: Insights From Ion-Pair Interactions. *Aust. J. Chem.* **2007**, *60*, 9−14.
(12) Zahn, S.; Thar, J.; Kirchner, B. Structure and Dynamics of the Protic Ionic Liquid Monomethylammonium Nitrate ([CH_3NH_3]-[NO_3]) from Ab Initio Molecular Dynamics Simulations. *J. Chem. Phys.* **2010**, *132*, No. 124506.
(13) Izgorodina, E. I. Towards Large-Scale, Fully Ab Initio Calculations of Ionic Liquids. *Phys. Chem. Chem. Phys.* **2011**, *13*, 4189−4207.
(14) Spohr, H. V.; Patey, G. N. Structural and Dynamical Properties of Ionic Liquids: Competing Influences of Molecular Properties. *J. Chem. Phys.* **2010**, *132*, 154504.
(15) Sarangi, S. S.; Reddy, S. K.; Balasubramanian, S. Low Frequency Vibrational Modes of Room Temperature Ionic Liquids. *J. Phys. Chem. B* **2011**, *115*, 1874−1880.
(16) Izgorodina, E. I.; MacFarlane, D. R. Nature of Hydrogen Bonding in Charged Hydrogen-Bonded Complexes and Imidazolium-Based Ionic Liquids. *J. Phys. Chem. B* **2011**, *115*, 14659−14667.
(17) Skarmoutsos, I.; Dellis, D.; Matthews, R. P.; Welton, T.; Hunt, P. A. Hydrogen Bonding in 1-Butyl- and 1-Ethyl-3-methylimidazolium Chloride Ionic Liquids. *J. Phys. Chem. B* **2012**, *116*, 4921−4933.
(18) Skarmoutsos, I.; Welton, T.; Hunt, P. A. The Importance of Timescale for Hydrogen Bonding in Imidazolium Chloride Ionic Liquids. *Phys. Chem. Chem. Phys.* **2014**, *16*, 3675−3685.
(19) Katsyuba, S. A.; Vener, M. V.; Zvereva, E. E.; Fei, Z.; Scopelliti, R.; Laurenczy, G.; Yan, N.; Paunescu, E.; Dyson, P. J. How Strong Is Hydrogen Bonding in Ionic Liquids? Combined X-ray Crystallographic, Infrared/Raman Spectroscopic, and Density Functional Theory Study. *J. Phys. Chem. B* **2013**, *117*, 9094−9105.
(20) Noda, A.; Susan, M. A. B. H.; Kudo, K.; Mitsushima, S.; Hayamizu, K.; Watanabe, M. Brønsted Acid-Base Ionic Liquids as Proton-Conducting Nonaqueous Electrolytes. *J. Phys. Chem. B* **2003**, *107*, 4024−4033.
(21) Susan, M. A. B. H.; Noda, A.; Mitsushima, S.; Watanabe, M. Brønsted acid-base ionic liquids and their use as new materials for anhydrous proton conductors. *Chem. Commun. (Cambridge, U. K.)* **2003**, 938−939.
(22) Nakamoto, H.; Watanabe, M. Brønsted acid-base ionic liquids for fuel cell electrolytes. *Chem. Commun. (Cambridge, U. K.)* **2007**, 2539−2541.
(23) Nakamoto, H.; Noda, A.; Hayamizu, K.; Hayashi, S.; Hamaguchi, H.-o.; Watanabe, M. Proton-Conducting Properties of a Brønsted Acid-Base Ionic Liquid and Ionic Melts Consisting of Bis(trifluoromethanesulfonyl)imide and Benzimidazole for Fuel Cell Electrolytes. *J. Phys. Chem. C* **2007**, *111*, 1541−1548.
(24) Lee, S.-Y.; Ogawa, A.; Kanno, M.; Nakamoto, H.; Yasuda, T.; Watanabe, M. Nonhumidified Intermediate Temperature Fuel Cells Using Protic Ionic Liquids. *J. Am. Chem. Soc.* **2010**, *132*, 9764−9773.
(25) Yasuda, T.; Ogawa, A.; Kanno, M.; Mori, K.; Sakakibara, K.; Watanabe, M. Hydrophobic Protic Ionic Liquid for Nonhumidified Intermediate-Temperature Fuel Cells. *Chem. Lett.* **2009**, *38*, 692−693.
(26) Yamamoto, K.; Tani, M.; Hangyo, M. Terahertz Time-Domain Spectroscopy of Imidazolium Ionic Liquids. *J. Phys. Chem. B* **2007**, *111*, 4854−4859.
(27) Stoppa, A.; Hunger, J.; Buchner, R.; Hefter, G.; Thoman, A.; Helm, H. Interactions and Dynamics in Ionic Liquids. *J. Phys. Chem. B* **2008**, *112*, 4854−4858.
(28) Daguenet, C.; Dyson, P. J.; Krossing, I.; Oleinikova, A.; Slattery, J.; Wakai, C.; Weingärtner, H. Dielectric Response of Imidazolium-Based Room-Temperature Ionic Liquids. *J. Phys. Chem. B* **2006**, *110*, 12682−12688.
(29) Turton, D. A.; Hunger, J.; Stoppa, A.; Hefter, G.; Thoman, A.; Walther, M.; Buchner, R.; Wynne, K. Dynamics of Imidazolium Ionic Liquids from a Combined Dielectric Relaxation and Optical Kerr Effect Study: Evidence for Mesoscopic Aggregation. *J. Am. Chem. Soc.* **2009**, *131*, 11140−11146.
(30) Nakamura, K.; Shikata, T. Systematic Dielectric and NMR Study of the Ionic Liquid 1-Alkyl-3-Methyl Imidazolium. *ChemPhysChem* **2010**, *11*, 285−294.
(31) Shirota, H.; Castner, E. W. Physical Properties and Intermolecular Dynamics of an Ionic Liquid Compared with Its Isoelectronic Neutral Binary Solution. *J. Phys. Chem. A* **2005**, *109*, 9388−9392.
(32) Xiao, D.; Rajian, J. R.; Hines, L. G.; Li, S.; Bartsch, R. A.; Quitevis, E. L. Nanostructural Organization and Anion Effects in the Optical Kerr Effect Spectra of Binary Ionic Liquid Mixtures. *J. Phys. Chem. B* **2008**, *112*, 13316−13325.
(33) Fujisawa, T.; Nishikawa, K.; Shirota, H. Comparison of interionic/intermolecular vibrational dynamics between ionic liquids and concentrated electrolyte solutions. *J. Chem. Phys.* **2009**, *131*, No. 244519.
(34) Dominguez-Vidal, A.; Kaun, N.; Ayora-Cañada, M. J.; Lendl, B. Probing Intermolecular Interactions in Water/Ionic Liquid Mixtures by Far-Infrared Spectroscopy. *J. Phys. Chem. B* **2007**, *111*, 4446−4452.
(35) Yokozeki, A.; Kasprzak, D. J.; Shiflett, M. B. Thermal effect on C-H stretching vibrations of the imidazolium ring in ionic liquids. *Phys. Chem. Chem. Phys.* **2007**, *9*, 5018−5026.
(36) Roth, C.; Chatzipapadopoulos, S.; Kerlé, D.; Friedriszik, F.; Lütgens, M.; Lochbrunner, S.; Kühn, O.; Ludwig, R. Hydrogen Bonding in Ionic Liquids Probed by Linear and Nonlinear Vibrational Spectroscopy. *New J. Phys.* **2012**, *14*, No. 105026.
(37) Wulf, A.; Fumino, K.; Ludwig, R.; Taday, P. F. Combined THz, FIR and Raman Spectroscopy Studies of Imidazolium-Based Ionic Liquids Covering the Frequency Range 2−300 cm^{-1}. *ChemPhysChem* **2010**, *11*, 349−353.
(38) Wulf, A.; Fumino, K.; Ludwig, R. Spectroscopic Evidence for an Enhanced Anion-Cation Interaction from Hydrogen Bonding in Pure Imidazolium Ionic Liquids. *Angew. Chem., Int. Ed.* **2010**, *49*, 449−453.
(39) Buffeteau, T.; Grondin, J.; Danten, Y.; Lassègues, J.-C. Imidazolium-Based Ionic Liquids: Quantitative Aspects in the Far-Infrared Region. *J. Phys. Chem. B* **2010**, *114*, 7587−7592.
(40) Grondin, J.; Lassègues, J.-C.; Cavagnat, D.; Buffeteau, T.; Johansson, P.; Holomb, R. Revisited Vibrational Assignments of Imidazolium-based Ionic Liquids. *J. Raman Spectrosc.* **2011**, *42*, 733−743.
(41) Hayes, R.; Imberti, S.; Warr, G. G.; Atkin, R. The Nature of Hydrogen Bonding in Protic Ionic Liquids. *Angew. Chem., Int. Ed.* **2013**, *52*, 4623−4627.
(42) Fumino, K.; Wulf, A.; Ludwig, R. The Cation-Anion Interaction in Ionic Liquids Probed by Far-Infrared Spectroscopy. *Angew. Chem., Int. Ed.* **2008**, *47*, 3830−3834.
(43) Wulf, A.; Fumino, K.; Ludwig, R. Comment on "New Interpretation of the CH Stretching Vibrations in Imidazolium-Based Ionic Liquids. *J. Phys. Chem. A* **2010**, *114*, 685−686.
(44) Fumino, K.; Fossog, V.; Wittler, K.; Hempelmann, R.; Ludwig, R. Dissecting Anion-Cation Interaction Energies in Protic Ionic Liquids. *Angew. Chem., Int. Ed.* **2013**, *52*, 2368−2372.
(45) Fumino, K.; Ludwig, R. Analyzing the Interaction Energies between Cation and Anion in Ionic Liquids: The Subtle Balance between Coulomb Forces and Hydrogen Bonding. *J. Mol. Liq.* **2014**, *192*, 94−102.
(46) Frisch, M. J.; Trucks, G. W.; Schlegel, H. B.; Scuseria, G. E.; Robb, M. A.; Cheeseman, J. R.; Scalmani, G.; Barone, V.; Mennucci, B.; et al. *Gaussian 09*, Revision D.01; Gaussian: Wallingford, CT, USA, 2009.
(47) Dennington, R.; Keith, T.; Millam, J. *GaussView*, Version 5; Semichem: Shawnee Mission, KS, USA, 2009.
(48) Hutter, J.; Ballone, J. P.; Bernasconi, M.; Focher, P.; Fois, E.; Goedecker, S.; Marx, D.; Parrinello, M.; Tuckerman, M. E. *CPMD*, Version 3.13.2; Max Planck Institut fuer Festkoerperforschung and IBM Zurich Research Laboratory: Stuttgart, Germany, and Zurich, Switzerland, 1990.

DOI: 10.1021/jp5113679
J. Phys. Chem. B 2015, 119, 1994−2002

(49) Troullier, N.; Martins, J. L. Efficient Pseudopotentials for Plane-wave Calculations. *Phys. Rev. B* **1991**, *43*, 1993−2006.
(50) Perdew, J. P.; Burke, K.; Ernzerhof, M. Generalized Gradient Approximation Made Simple. *Phys. Rev. Lett.* **1996**, *77*, 3865−3868.
(51) Grimme, S. Semiempirical GGA-type Density Functional Constructed with a Long-Range Dispersion Correction. *J. Comput. Chem.* **2006**, *27*, 1787−1799.
(52) Hockney, R. W. A Fast Direct Solution of Poisson's Equation Using Fourier Analysis. *J. Assoc. Comput. Mach.* **1965**, *12*, 95−113.
(53) Allen, F. H. The Cambridge Structural Database: A Quarter of a Million Crystal Structures and Rising. *Acta Crystallogr., Sect. B: Struct. Sci.* **2002**, *58*, 380−388.
(54) Bruno, I. J.; Cole, J. C.; Edgington, P. R.; Kessler, M.; Macrae, C. F.; McCabe, P.; Pearson, J.; Taylor, R. New Software for Searching the Cambridge Structural Database and Visualizing Crystal Structures. *Acta Crystallogr., Sect. B: Struct. Sci.* **2002**, *58*, 389−397.
(55) Bruno, I.; Cole, J.; Lommerse, J.; Rowland, R.; Taylor, R.; Verdonk, M. IsoStar: A Library of Information About Nonbonded Interactions. *J. Comput.-Aided Mol. Des.* **1997**, *11*, 525−537.
(56) Plimpton, S. Fast Parallel Algorithms for Short-Range Molecular Dynamics. *J. Comput. Phys.* **1995**, *117*, 1−19.
(57) Canongia Lopes, J. N.; Pádua, A. A. H. Molecular Force Field for Ionic Liquids Composed of Triflate or Bistriflylimide Anions. *J. Phys. Chem. B* **2004**, *108*, 16893−16898.
(58) Hoover, W. G. Canonical Dynamics: Equilibrium Phase-space Distributions. *Phys. Rev. A* **1985**, *31*, 1695−1697.
(59) Krishnan, M.; Balasubramanian, S. Vibrational Dynamics of Solid Poly(ethylene oxide). *Phys. Rev. B* **2003**, *68*, No. 064304.
(60) Martyna, G. J.; Klein, M. L.; Tuckerman, M. Nosé-Hoover Chains: The Canonical Ensemble via Continuous Dynamics. *J. Chem. Phys.* **1992**, *97*, 2635−2643.
(61) Macrae, C. F.; Edgington, P. R.; McCabe, P.; Pidcock, E.; Shields, G. P.; Taylor, R.; Towler, M.; van de Streek, J. *Mercury*: Visualization and Analysis of Crystal Structures. *J. Appl. Crystallogr.* **2006**, *39*, 453−457.
(62) Humphrey, W.; Dalke, A.; Schulten, K. VMD: Visual Molecular Dynamics. *J. Mol. Graphics* **1996**, *14*, 33−38.
(63) Jmol: An open-source Java viewer for chemical structures in 3D. http://www.jmol.org/.
(64) Sebastiani, D.; Parrinello, M. A New ab-Initio Approach for NMR Chemical Shifts in Periodic Systems. *J. Phys. Chem. A* **2001**, *105*, 1951−1958.
(65) Sebastiani, D.; Goward, G.; Schnell, I.; Parrinello, M. NMR Chemical Shifts in Periodic Systems from First Principles. *Comput. Phys. Commun.* **2002**, *147*, 707−710.
(66) Sebastiani, D.; Parrinello, M. Ab-Initio Study of NMR Chemical Shifts of Water Under Normal and Supercritical Conditions. *ChemPhysChem* **2002**, *3*, 675−679.
(67) Goward, G. R.; Schuster, M. F. H.; Sebastiani, D.; Schnell, I.; Spiess, H. W. High-Resolution Solid-State NMR Studies of Imidazole-Based Proton Conductors: Structure Motifs and Chemical Exchange from ^{1}H NMR. *J. Phys. Chem. B* **2002**, *106*, 9322−9334.
(68) Goward, G. R.; Sebastiani, D.; Schnell, I.; Spiess, H. W.; Kim, H.-D.; Ishida, H. Benzoxazine Oligomers: Evidence for a Helical Structure from Solid-State NMR Spectroscopy and DFT-Based Dynamics and Chemical Shift Calculations. *J. Am. Chem. Soc.* **2003**, *125*, 5792−5800.
(69) Manz, T. A.; Sholl, D. S. Improved Atoms-in-Molecule Charge Partitioning Functional for Simultaneously Reproducing the Electrostatic Potential and Chemical States in Periodic and Nonperiodic Materials. *J. Chem. Theory Comput.* **2012**, *8*, 2844−2867.
(70) Manz, T. A.; Sholl, D. S. Chemically Meaningful Atomic Charges That Reproduce the Electrostatic Potential in Periodic and Nonperiodic Materials. *J. Chem. Theory Comput.* **2010**, *6*, 2455−2468.
(71) Mondal, A.; Balasubramanian, S. Quantitative Prediction of Physical Properties of Imidazolium Based Room Temperature Ionic Liquids through Determination of Condensed Phase Site Charges: A Refined Force Field. *J. Phys. Chem. B* **2014**, *118*, 3409−3422.

DOI: 10.1021/jp5113679
J. Phys. Chem. B 2015, 119, 1994−2002